JOURNAL OF CATALYSIS 132, 1–20 (1991)

Deactivation in Catalytic Hydrodemetallation

I. Model Compound Kinetic Studies

BARBARA J. SMITH[1] AND JAMES WEI

Department of Chemical Engineering, Massachusetts Institute of Technology, Cambridge, Massachusetts 02139

Received November 2, 1989; revised May 22, 1991

Model compound hydrodemetallation (HDM) studies are used to examine the effect of accumulating metal-sulfide deposits on catalyst deactivation in a clean reactant system. Experiments are carried out in a catalyst-slurry batch reactor, using a sulfided $CoMo/Al_2O_3$ catalyst and a low-promoter alumina carrier. The model compounds are nickel etioporphyrin (Ni-EP) and vanadyl etioporphyrin (VO-EP). Standard experimental conditions are 320°C, 4.8 MPa total pressure, and 14 kPa hydrogen sulfide. Ni-EP HDM studies carried out with the sulfided $CoMo/Al_2O_3$ catalyst operating in the kinetic regime show that, contrary to expectations, the catalyst does not deactivate significantly as it accumulates nickel-sulfide deposits to levels as high as 100 wt% Ni. Ni-EP HDM studies carried out with a low-promoter alumina carrier show that the carrier has a low level of catalytic activity, and neither deactivates nor acquires catalytic activity as nickel-sulfide deposits accumulate to 25 wt% Ni. The relative activity for the two catalysts matches the relative promoter loadings. VO-EP HDM studies carried out under diffusion-limited conditions with the $CoMo/Al_2O_3$ catalyst show that it deactivates steadily as vanadium-sulfide deposits accumulate. Both the reactivity and the apparent effective diffusivity of VO-EP on the sulfided catalyst are significantly lower than those of Ni-EP.

1. INTRODUCTION

The upgrading of heavy residuum oils will continue to increase in importance as changes in crude oil availability cause a shift toward heavier crudes. For very heavy crudes, the bottom residuum fraction may contain significant quantities of metals, mainly nickel, vanadium, and iron, as well as sulfur and nitrogen heteroatoms. The metals pose a particular problem for refiners because metal contaminants accumulate on catalysts during hydrotreating causing permanent catalyst deactivation. For this reason, hydroprocessing schemes often use hydrodemetallation (HDM) catalysts to remove metals selectively and protect downstream catalysts.

Typically an S-shaped catalyst deactivation profile is observed during hydrodemetallation. An initial period of rapid deactivation is generally attributed to the establishment of an equilibrium coke loading on the catalyst (*1–4*), but has also been attributed to the buildup of a monolayer or submonolayer of metal deposits on the catalyst surface (*5*). An intermediate deactivation period, characterized by a slow and almost constant deactivation rate, is usually ascribed to increasing diffusional resistance as metal-sulfide deposits accumulate in the pores, or to a decline in catalyst activity. The final, rapid deactivation that brings the catalyst to the end of its working life is attributed to pore plugging caused by the accumulation of metal-sulfide deposits.

The precise role of metal-sulfide deposits in determining catalyst activity and the effective diffusivity of reactant molecules has not been well established. In modeling catalyst deactivation, it is commonly postulated that metal sulfides accumulate in a uniform manner at the microscopic scale, building

[1] Present address: Chevron Research and Technology Company, Richmond, CA 94802.

0021-9517/91 $3.00

up layer by layer and effectively blocking access to the surface of the catalyst after the deposition of just one monolayer-equivalent. Catalytic activity is subsequently due to the intrinsic activity of the deposited metal sulfides. Evidence for this catalytic effect comes from studies that show that bare aluminas gradually acquire catalytic activity for removing metals from a residual feedstock when exposed to the feedstock under hydroprocessing conditions (*2, 6*). However, the model of locally uniform deposition has not been demonstrated directly by examination of the catalyst surface.

The objective of this work was to investigate the effects of nickel- and vanadium-sulfide deposits on the activity of two catalysts, in a clean model-compound reactant system. Our model compounds were metalloporphyrins, which have been used previously in model-compound studies (*7–13*). Specifically, we addressed the following questions:

- What is the mechanism of nickel etioporphyrin (Ni-EP) and vanadyl etioporphyrin (VO-EP) hydrodemetallation over sulfided catalysts?
- What are the relative reactivities and diffusivities of Ni-EP and VO-EP?
- What are the relative activities and selectivities of a $CoMo/Al_2O_3$ catalyst and a low-promoter alumina carrier?
- How do the catalysts deactivate as nickel- and vanadium-sulfide deposits accumulate?

2. EXPERIMENTAL AND MATHEMATICAL METHODS

2.1. Materials

The model compounds used in this investigation were nickel and vanadyl etioporphyrin. Some experiments were run using the partially hydrogenated reaction intermediate nickel etiochlorin (Ni-EPH_2). The porphyrins and the chlorin were purchased from Midcentury Chemicals (Posen, IL). Nickel and vanadyl etioporphyrin were selected as model compounds because they are representative of the porphyrinic species found in crude oils. The nonporphyrinic metal fraction is comprised of compounds with less-well-characterized structures and properties, a considerable pecentage of which are complexed to large-molecular-weight species that precipitate with the asphaltene fraction (*14*). The nonporphyrinic fraction is thus less amenable to model compound studies.

Squalane (2,6,10,15,19,23-hexamethyltetracosane) was used as a carrier oil in all the studies reported here. It was supplied by Sigma Chemical Co. (St. Louis, MO). Squalane was selected as a solvent because it meets several important criteria: it is free of sulfur, nitrogen, and metal compounds; it is a liquid at room temperature; and it has a relatively high boiling point so the vapor pressure of the oil is negligible at reaction conditions. Squalane is an isoparaffin. Analysis shows that it contains 1.75 wt% polynaphthenes and 0.85 wt% aromatics. The important properties of squalane are summarized in Table 1. A limited number of experiments were conducted using Kaydol, a commercial mineral oil supplied by Ruger Chemical Co. (Irvington, NJ). Kaydol is a mixture of hydrocarbons consisting primarily of naphthenes, but containing 22.3 wt% paraffins and 4.1 wt% aromatics.

The solubility of the porphyrins in squalane is relatively low at room temperature, about 20 ppm metal. However, at reaction temperatures the solubilities are much higher. At a temperature of 320°C, the solubility limit was not reached at dissolved porphyrin concentrations up to 300 ppm metal. In Kaydol the solubility of both Ni-EP and VO-EP is about 40 ppm metal at room temperature.

The principal catalyst used in this study was American Cyanamid Aero HDS16A, a $CoMo/Al_2O_3$ catalyst supplied in the oxide form as $\frac{1}{16}$-in. extrudates. The properties of this catalyst are summarized in Table 2. HDS16A has a unimodal pore-size distribution with a median pore diameter of 8.04 nm (80.4 Å). It has been superceded in commer-

TABLE 1

Squalane Properties

Supplier: Sigma Chemical Co., St. Louis, MO	
Lot Number: 116F-0221	
Chemical formula: 2,6,10,15,19, 23-hexamethyltetracosane	
Molecular weight: 422.8	
Properties: (courtesy of Mobil Research & Dev. Corp., Paulsboro NJ)	
Sulfur	<1 ppm
Nitrogen	1 ppm
Nickel	0.25 ppm
Vanadium	<0.05 ppm
Hydrogen	15.29 wt%
Density at 25°C	0.806 g/cc
P/N/A Distribution (wt%)	
Paraffins	97.40
Mononaphthenes	0.00
Polynaphthenes	1.75
Aromatics	0.85
Simulated distillation by GC	
IBP	414°C
50%	431°C
90%	435°C
95%	436°C
FBP	443°C

cial applications, but is retained for our model-compound investigation because its unimodal pore-size distribution makes the investigation of reaction and diffusion effects more straightforward. Kinetic studies were carried out with crushed catalyst particles, generally in the size range 75–88 μm (170–200 ASTM mesh). Analysis of the crushed catalyst (see Table 2) indicates that the milling and sieving operations did not significantly alter the physical properties of the catalyst. In all the experiments in this investigation the catalyst was presulfided before use.

Additional investigations were made using a low-promoter alumina carrier, American Cyanamid HDS3 substrate, which had been taken from the manufacturing process before metals impregnation. It is a porous (unimodal) gamma-alumina carrier with low levels of molybdenum, cobalt, nickel, and phosphorous promoters. This is the closest available material to Cyanamid HDS16A substrate, which is no longer manufactured. The properties of HDS3 substrate are summarized in Table 2. It was calcined at 480°C and presulfided before use.

2.2. *Apparatus*

Two catalyst-slurry batch reactors were used for the hydrodemetallation studies. Most experiments were carried out in a 1-liter stirred autoclave, described previously by Hung and Wei (*7*). Subsequent modifications include the addition of an improved temperature control system, a catalyst sulfiding system, and a 1-liter feed preheater. Details of these modifications are given by Smith (*15*). A reactor system based around a 2-liter stirred autoclave was used in the low-promoter alumina carrier experiments. This reactor is described fully by Limbach (*16*). The most important difference is that it did not have a feed preheater.

2.3. *Experimental*

The hydrodemetallation experimental series described in this paper are summarized in Table 3. Model-compound hydrodesulfurization and hydrogenation experiments using dibenzothiophene and naphthalene were carried out as additional experiments during some of these series. These experiments are described by Rautiainen and Wei (*17*). Typically, multiple batch experiments were carried out on each charge of catalyst, to allow the monitoring of activity as metal-sulfide deposits accumulated on the catalyst.

For each experimental series, catalyst pretreatment consisted of drying overnight at 110°C, slurrying in oil in the autoclave reactor, and sulfiding *in situ*. Sulfiding was carried out according to a standard procedure recommended by American Cyanamid. The catalyst was heated to 175°C under a flow of helium (99.995% purity, Matheson Gas Products). Sulfiding was achieved with a mixture of 10 mol% H_2S/H_2 (Matheson Gas Products) flowing at a rate of

TABLE 2

Catalyst Properties

	$CoMo/Al_2O_3$ Catalyst	Low-promoter alumina carrier
	AERO HDS16A[a] Lot Number: MTG-S-0573	HDS3 Substrate[a,b] (calcined at 480°C)
	Chemical properties[c]	
Mo	8.1 wt% (dry basis)	0.24 wt% (dry basis)
Co	4.5 wt%	0.68 wt%
P	3.00 wt%	0.18 wt%
Ni	0.09 wt%	0.32 wt%
Si	0.15 wt%	0.25 wt%
Na	0.02 wt%	NA
Fe	0.04 wt%	NA
γ-Al_2O_3	Base	Base
	Physical properties[d]	
Crushed catalyst (170–200 mesh, 75–88 μm)		
Pore volume	0.44 ml/g	0.65 ml/g (Unocal)
Surface area	177 m^2/g	258 m^2/g (Unocal)
Med. pore diameter		
Vol, N_2 des.	85.3 Å (Unocal)	82.4 Å (Unocal)
Area, Hg	97 Å (Unocal)	79.8 Å (Unocal)
Extrudates		
Average diameter	0.152 cm ($\frac{1}{16}$ in.)	
Average length	0.432 cm	
Pore volume	0.43 ml/g	
Surface area	176 m^2/g	
Particle density	1.49 g/ml	
Median pore diameter:		
Vol	80.4 Å (Cyanamid)	
Vol, N_2 des.	86.9 Å (Unocal)	
Area, Hg	96 Å (Unocal)	

[a] Supplier: American Cyanamid Co., Stamford, CT.
[b] Taken from the manufacturing process before metals impregnation.
[c] From American Co. for AERO HDS16A. Analysis by Galbraith for HDS3 Substrate.
[d] From American Cyanamid Co. and Unocal. Corp.

at least 100 cc/min, according to a standard temperature program. The temperature was held at 175°C for 6 h, then raised to 315°C at 60°C/h, then maintained at 315°C for 1 h. Experiments showed very little difference in initial activity between a catalyst sample sulfided under gas flow prior to addition to the reactor and the samples sulfided *in situ*.

Operating conditions for the HDM experiments ranged from 280 to 350°C at hydrogen pressures of 1–8.3 MPa (300–1200 psig). The standard conditions for monitoring changes in catalyst activity were 320°C and 4.8 MPa (700 psig). For each experiment a H_2S partial pressure of about 14 kPa (0.3 vol%) was maintained in the reactor. In fact, the control of H_2S partial pressure was not very precise, and this parameter varied from 10 to 35 kPa. No significant dependence of HDM reaction rate on H_2S partial pressure

TABLE 3

Summary of HDM Experiments

Series	Catalyst	Conditions	Reactant[a]	Experiment
SA11	$CoMo/Al_2O_3$ 75–88 μm 1.1 g	280–350°C 4.8 MPa 14 kPa H_2S	Ni-EP	Multiple batch experiments, to 20 wt% Ni
SA12	$CoMo/Al_2O_3$ 75–88 μm 1.0 g	320°C 2.1–8.3 MPa 14 kPa H_2S	Ni-EP	Multiple batch experiments, to 60 wt% Ni
AL13	Al_2O_3 (low levels of promoter) 75–88 μm 3.1 g	320°C 4.8 MPa 5 kPa H_2S	Ni-EP	Multiple batch experiments, to 25 wt% Ni
SA15	$CoMo/Al_2O_3$ 300–350 μm 1.0 g	320°C 4.8 MPa 14 kPa H_2S	Ni-EP	Single batch experiment, to 10 wt% Ni
SA17	$CoMo/Al_2O_3$ 75–88 μm 1.0 g	320°C 4.8 MPa 14 kPa H_2S	VO-EP	Multiple batch experiments, to 25 wt% V
SA18	$CoMo/Al_2O_3$ 75–88 μm 0.1 g	320°C 4.8 MPa 14 kPa H_2S	Ni-EPH_2 Ni-EP	—Single expt. —Single expt. to 100 wt% Ni
SA19	$CoMo/Al_2O_3$ 37–44 μm 1.1 g	320°C 4.8 MPa 14 kPa H_2S	VO-EP	Single batch experiment, to 4 wt% V

[a] Solvent for all experiments was Squalane.

was found within this range, although higher H_2S pressures did seem to enhance observed HDM rates.

Prior to each kinetic experiment the reactor and preheater were pressurized with a 10 mol% H_2S/H_2 gas mixture and then pure hydrogen to pressures that would achieve the desired H_2S partial pressure and hydrogen total pressure at reaction temperature. Each experiment was initiated by the rapid injection from the preheater of a slurry of the feed model compound in approximately 50 g of oil. The feed was heated to reaction temperature prior to addition. Tests showed that any porphyrin undissolved at the time of feed addition was rapidly dissolved in the reactor. No undissolved porphyrin was present by the time the first liquid samples were taken.

Each experiment was monitored by analysis of liquid samples of approximately 1 g (preceded by a 2 g purge of the sample line), taken periodically. At the conclusion of each experiment the reactor temperature was maintained at around 320°C, but the reactor was vented to atmospheric pressure and purged with the H_2S/H_2 mixture to ensure that no light reaction products were carried over to the next experiment. Gas samples were taken to monitor H_2S levels. In general, 15–20% of the total volume of oil in the reactor was replaced with the feed for a subsequent experiment. Occasionally the oil was changed completely between experiments. With squalane as a solvent there was no difference in the observed rate constants if a fraction of the oil was retained from the previous experiment.

Up to 20 batch experiments were performed with a given catalyst, to allow the monitoring of catalyst activity as metal accumulated. At the conclusion of a series of experiments the catalyst was allowed to settle. The reactor was disassembled and the catalyst transferred in the autoclave glass liner, under cover of oil, to an Argon glove

box. The catalyst was filtered from the oil, rinsed repeatedly with xylene (Fisher Scientific), and dried in a self-sealing quartz crucible (Fisher Scientific) prior to analysis. The catalyst was heated overnight in a vacuum oven prior to pore-size distribution, surface area, and elemental analysis.

HDM experiments carried out with no catalyst in the reactor confirmed that the thermal reaction rate is very slow relative to the catalytic rate. Experiments carried out with catalyst to oil weight ratios varied over an order of magnitude showed no sensitivity to this parameter, provided it was properly accounted for in the reaction rate constants.

The second reactor-system was only used for the relatively slow low-promoter alumina-carrier experiments. This reactor did not have a preheater so feed was added at low temperature (60–70°C) with the reactor open to the atmosphere. The reactor was purged with helium, hydrogen, and a 10 mol% H_2S/H_2 mixture (100 cc/min, each for 30 min) before pressurization to the desired H_2S partial pressure and total H_2 pressure. It was then heated to reaction temperature as rapidly as possible. Generally a 3-h heat-up period was necessary before isothermal data could be taken. Because the alumina-carrier experiments were relatively slow (of minimum duration 25 h), this initial temperature transient was not significant.

2.4. *Analysis*

Liquid samples were diluted by xylene (Fisher Scientific) and routinely analyzed by ultraviolet visible spectrophotometry (Bausch and Lomb Spectronic 2000). Calibration factors for the porphyrinic species were 0.478 Abs/ppm Ni for Ni-EP (552 nm), 0.72 Abs/ppm Ni for Ni-EPH_2 (616 nm), 0.56 Abs/ppm V for VO-EP (570.5 nm), and 0.61 Abs/ppm V for VO-EPH_2 (631 nm) (*8, 11*). In some exceptional cases it was necessary to use a nonlinear calibration curve, because samples had not been diluted sufficiently to be in the linear regime. Atomic absorption spectrophotometry (Perkin–Elmer 360) was used to determine total nickel and vanadium concentrations.

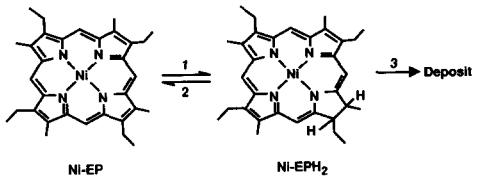

FIG. 1. HDM reaction sequence for nickel etioporphyrin.

Gas samples were collected in a 100-cc glass sample cylinder at the conclusion of each experiment. Gas samples of 0.1 ml were routinely analyzed for hydrogen sulfide and ammonia concentrations using gas detector tubes (Kitagawa, Japan, H_2S 1-150 ppm, NH_3 5-260 ppm).

Radial nickel and vanadium profiles in the catalyst particles were obtained using an electron microprobe (Cameca Microbeam). Catalyst particles were embedded in resin and ground down so that the particle cross section was exposed. The final surface polishing was done with 0.3-μm abrasive paper. In some cases electron microprobe analyses were made directly from resin-embedded catalyst particles that had been sectioned by ultramicrotoming during sample preparation for transmission electron microscopy. This procedure and elemental compositions of the spent catalysts are reported in full in the following paper in this series (*18*). Metal analysis was by atomic absorption spectroscopy, and carbon analysis was by microcombustion.

2.5. *Mathematical Modeling of Kinetics and Diffusion in Etioporphyrin HDM*

Hydrodemetallation kinetics for Ni-EP and VO-EP on unsulfided $CoMo/Al_2O_3$ were first reported by Agrawal and Wei (*8*) to proceed via a sequential mechanism. As shown in Fig. 1, a reversible hydrogenation of the porphyrin (Ni-EP) to form the etiochlorin (Ni-EPH_2) is followed by an irre-

versible hydrogenolysis that results in the fragmentation of the porphyrin ring and deposition of the metal on the catalyst. An identical mechanism was proposed for VO-EP. The matrix equations describing the etioporphyrin reaction scheme, and the extension to the case of coupled reaction and diffusion have been presented previously (*8, 19*).

For batch experiments a contact time, $\hat{t}$, is defined

$$\hat{t} = \frac{W_c}{W_{oil}} t, \tag{1}$$

where W_{oil} is the weight of oil in the reactor, and W_c is the weight of catalyst. For batch experiments $\hat{t}$ is corrected for the changes in the weight of oil in the reactor as a consequence of sampling. The matrix rate equation for the etioporphyrin reaction system can be written

$$\frac{d\mathbf{C}}{d\hat{t}} = -\bar{\mathbf{K}}\mathbf{C}$$

or

$$\frac{d}{d\hat{t}}\begin{bmatrix} C_2 \\ C_2 \end{bmatrix} = -\begin{bmatrix} k_1 & -k_2 \\ -k_1 & k_2 + k_3 \end{bmatrix}\begin{bmatrix} C_1 \\ C_2 \end{bmatrix}, \tag{2}$$

where C_1 and C_2 are the concentrations of Ni-EP and Ni-EPH$_2$, respectively. The rate constants are expressed in units g oil/g cat h. Constant hydrogen concentration in the oil is assumed. The eigenvalues of the rate matrix, $\bar{\mathbf{K}}$, give the two characteristic "time constants" for reaction. A "fast" eigenvalue, λ_{fast}, describes the buildup in concentration of the reaction intermediate, and a "slow" eigenvalue, λ_{slow}, describes the decline in concentration of both species.

$$\lambda_{fast} = \frac{(k_1 + k_2 + k_3) + \sqrt{(k_1 + k_2 + k_3)^2 - 4k_1k_3}}{2} \tag{3}$$

$$\lambda_{slow} = \frac{(k_1 + k_2 + k_3) - \sqrt{(k_1 + k_2 + k_3)^2 - 4k_1k_3}}{2}. \tag{4}$$

The solution to Eq. (2) for an initial condition $\mathbf{C} = \mathbf{C}_0$ is given by

$$\mathbf{C} = \bar{\mathbf{X}}\begin{bmatrix} \exp(-\lambda_{slow}\hat{t}) & 0 \\ 0 & \exp(-\lambda_{fast}\hat{t}) \end{bmatrix}\bar{\mathbf{X}}^{-1}\mathbf{C}_0, \tag{5}$$

where $\bar{\mathbf{X}}$ is the eigenvector matrix of the rate matrix, $\bar{\mathbf{K}}$.

Equation (5) was used to evaluate intrinsic kinetic parameters from experimental data using a nonlinear least-squares minimization routine. The Nelder–Mead simplex algorithm was used for function minimization (*20*). Usually, the selectivity ratios k_2/k_1 and k_3/k_1 were estimated independently, and the nonlinear least-squares algorithm was used to fit a single parameter, k_1 for each set of batch data.

In the case of diffusion-limited HDM the theory of coupled multicomponent reaction and diffusion given by Wei (*21*) can be used to model the diffusion-disguised reaction kinetics and to describe the concentration profiles in the catalyst particles as a function of time. The solution of the coupled reaction and diffusion equations is of the same form as Eq. (*5*), but the apparent eigenvalues and rate constants are diffusion-disguised.

The metal deposition profile in the catalyst particles can be calculated from the reactant concentration profiles. The approach used for calculating metal deposition profiles in particles from a packed bed reactor, for which the bulk concentrations at any given axial location are steady with time, has been given previously (*8, 19*). For metal deposition profiles generated in a batch reactor, a quasi steady-state approximation is made to take account of the decline of bulk concentrations with time. The details of this approach are given by Smith (*15*). We assume the effective diffusivities for the etioporphyrin and the etiochlorins to be equal, since the experimental data provide no basis for assuming otherwise. If the intrinsic rate constants are known, the effective diffusivity is determined by fitting a calculated metal

deposition profile to the experimental profile.

3. HDM OF Ni-EP IN SQUALANE OVER $CoMo/Al_2O_3$

Three series of experiments were carried out to determine Ni-EP hydrodemetallation kinetics and to investigate catalyst deactivation by monitoring the changes in observed kinetics as nickel-sulfide deposits accumulated on the $CoMo/Al_2O_3$ catalyst. In addition, a single experiment was run under diffusion-limited conditions to evaluate the effective diffusivity of Ni-EP in the sulfided $CoMo/Al_2O_3$ catalyst. The standard conditions for all experiments were 320°C, 4.8 MPa total pressure, and 14 kPa H_2S.

Reaction Kinetics

As discussed above, the sequential reaction scheme for EP hydrodemetallation has three adjustable parameters (the rate constants for hydrogenation, dehydrogenation, and hydrogenolysis: k_1, k_2, and k_3), but only two characteristic modes (λ_{fast} and λ_{slow}). If experiments were run using only Ni-EP as a feed it would be difficult to distinguish between kinetic models based on very different sets of the three rate constants. The best way to ensure an accurate kinetic model is to obtain an independent assessment of the reaction selectivities by running an experiment using the intermediate Ni-EPH_2 as a feed. We used this approach. We also ran experiments at many different Ni-EP feed concentrations to investigate the effect of that variable.

We ran three series of kinetic experiments (SA11, SA12, SA18) with catalyst particles in the size range 75–88 μm (170–200 ASTM mesh). Nickel loadings achieved in these series were 20 wt% Ni, 60 wt% Ni, and 100 wt% Ni, respectively. The catalyst charge was approximately 1 g for series SA11 and SA12, and 100 mg for series SA18. Series SA11 and SA12 consisted of multiple batch experiments, which were run sequentially at starting concentrations that varied over an order of magnitude, from 20 ppm Ni to 300 ppm Ni, adding nickel to the catalyst in increments of about 0.5 to 5 wt% Ni. Series SA18 consisted of a single kinetic experiment followed by a deactivation experiment in which the catalyst was loaded from 8 to 100 wt% Ni.

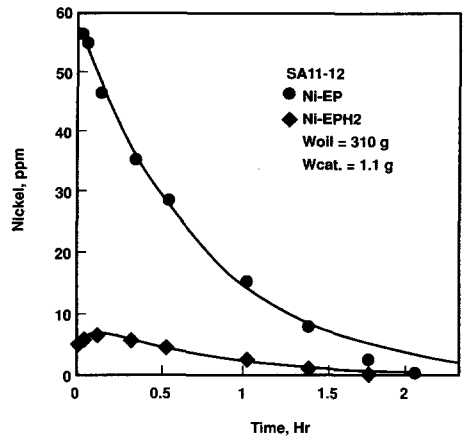

FIG. 2. Typical concentration versus time results for a single hydrodemetallation experiment with Ni-etioporphyrin at 320°C, 4.8 MPa H_2, on the $CoMo/Al_2O_3$ catalyst. Solid lines represent model calculations.

Figure 2 shows the variation in reactor concentrations as a function of time for a typical experiment using Ni-EP as a feed. Initially there was a buildup of Ni-EPH_2, followed by a decline in concentration of both the Ni-EP and Ni-EPH_2 species. Atomic absorption analysis of total nickel levels in the oil confirmed that the two porphyrins accounted for all the nickel-containing species present.

Figure 3 shows concentrations as a function of time for an experiment using pure Ni-EPH_2 as a feed. In the time taken to get the reactor to stable conditions there was a rapid increase in the concentration of Ni-EP, as it was formed from Ni-EPH_2. This observation suggests that the rate of the dehydrogenation reaction (k_2) was significant relative to the hydrogenation reaction (k_1). A pool of Ni-EP accumulated, which suggests that hydrogenation of Ni-EP to Ni-

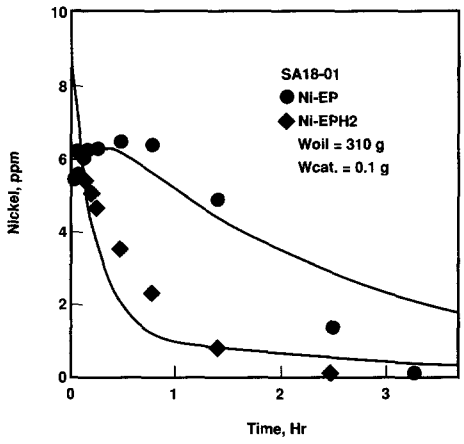

FIG. 3. Concentration versus time results for a single hydrodemetallation experiment with Ni-etiochlorin at 320°C, 4.8 MPa H_2, on the $CoMo/Al_2O_3$ catalyst. Solid lines represent model calculations.

EPH_2 (k_1) was slower than the hydrogenolysis of Ni-EPH_2 (k_3). At long times the decline in concentration of both Ni-EP and Ni-EPH_2 resembled the case in which Ni-EP was the feed.

We found the best-fit reaction selectivities for Ni-EP HDM by jointly minimizing over data from the Ni-EP and Ni-EPH_2 feed experiments. They were $k_2/k_1 = 2.0$ and $k_3/k_1 = 4.7$. Thus the hydrogenation of Ni-EP (k_1) is the rate-limiting step in the overall demetallation scheme, and the hydrogenolysis of Ni-EPH_2 (k_3) is the most rapid step. The solid line model results in both Fig. 2 and Fig. 3 were calculated using these selectivities.

A total of 21 sets of data were available from the experiments run on catalysts SA11 and SA12. We found a consistent fit to the data with the set of rate constants based on $k_2/k_1 = 2.0$ and $k_3/k_1 = 4.7$. Thus we concluded that there was no change in the selectivity of the $CoMo/Al_2O_3$ catalyst with the accumulation of nickel-sulfide deposits. Consequently a single parameter, k_1, is used to characterize each experiment.

Analysis of the effect of initial concentration on the Ni-EP hydrogenation rate constant k_1 is summarized in Fig. 4. For a simple first-order reaction network we would expect the calculated rate constants to be independent of feed concentration. However, varying feed concentration over an order of magnitude from 20 to 300 ppm Ni, we observe an inverse dependence of rate constant k_1 on feed concentration. Similar observations have been made previously by Agrawal (*22*), who used the etioporphyrins and an unsulfided catalyst. An explanation is provided by a Langmuir–Hinshelwood analysis of the adsorption/reaction process, assuming surface reaction to be rate controlling and no change in the number of active sites during the course of reaction. The conclusion from this analysis is that adsorption of Ni-EP, Ni-EPH_2, and hydrogenolysis products (shown by Ware and Wei (*11*) to be porphyrin ring fragments) is significant, and the adsorption constants for all species are similar. Letting k_{1s} be the surface reaction rate constant, S_0 the total number of active sites, and M_0 the initial porphyrin concentration (Ni-EP + Ni-EPH_2), the kinetic expression for the hydrogenation reaction step is

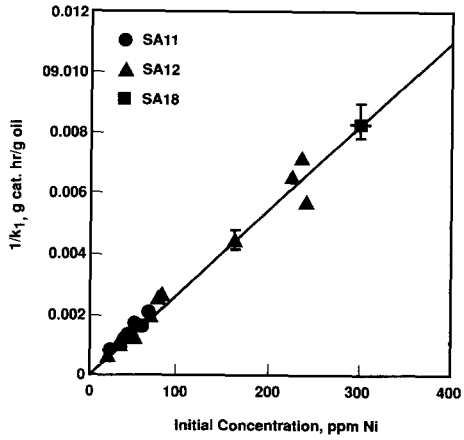

FIG. 4. Hydrogenation rate constant, k_1, shows an inverse dependence on feed concentration, at 320°C, 4.8 MPa H_2.

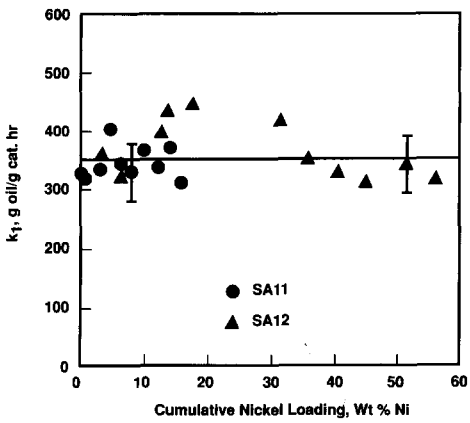

FIG. 5. Hydrogenation rate constant for Ni-EP hydrodemetallation, k_1, versus cumulative nickel loading on the $CoMo/Al_2O_3$ catalyst. Rate constant adjusted to initial Ni-EP concentration of 100 ppm Ni. Conditions: 320°C, 4.8 MPa H_2.

$$k_1 = \frac{k_{1s} S_0 P_{H_2}}{M_0} \tag{6}$$

$$k_{1s} = \frac{k_1 M_0}{S_0 P_{H_2}}. \tag{7}$$

Throughout this paper, all Ni-EP HDM rate constants are corrected for this dependence on feed concentration, and reported at a standard value of 100 ppm Ni.

Temperature-dependence experiments for Ni-EP hydrodemetallation are detailed in Smith (*15*). The Arrhenius activation energies for the hydrogenation (k_1), dehydrogenation (k_2), and hydrogenolysis (k_3) steps were all in the range 20–22 kcal/mole. These are comparable with the values reported by Ware and Wei (*11*) for the hydrodemetallation of Ni-EP on an unsulfided $CoMo/Al_2O_3$ catalyst, except that they report a higher activation energy (28.7 kcal/mol) for hydrogenolysis (k_3).

Catalyst Deactivation

A compilation of the rate constants from all the Ni-EP in squalane HDM experiments run at standard conditions on the $CoMo/Al_2O_3$ catalyst is given in Fig. 5. The nickel loadings on the catalyst are reported as wt% Ni on a fresh catalyst basis. Nickel loadings are calculated by mass balance for each experiment. The results of elemental analyses of catalyst particles removed from the reactor at the conclusion of each experimental run are given in Table 1 of the following paper (*18*). Nickel analysis results confirm the mass balance calculations. Carbon levels are relatively low (about 5 wt% for catalysts aged with a model-compound feed based on squalane) on all catalyst samples. There is evidence that the carbon builds up rapidly, in a time scale shorter than that for nickel accumulation (*18*). Thus the accumulation of carbonaceous deposits is not thought to be significant in the results discussed here.

The scatter in the rate constants in Fig. 5 reflects the difficulties associated with running multiple batch experiments on a single charge of catalyst. Nevertheless, the slope of a line regressed through the data does not differ significantly from zero, at the 95% confidence interval. This means that catalyst HDM activity remains constant in the presence of up to 60 wt% Ni on the catalyst, a remarkable result. We describe the data with the mean value for k_1, which is 350 g oil/g cat h at a feed concentration of 100 ppm Ni.

Based on the density of the fresh catalyst (1.49 g/ml), the density of nickel sulfide (5.82 g/ml for Ni_3S_2, see (*18*) for assignment of this phase), and the catalyst void fraction (0.64), a simple calculation shows that at a metal loading of 60 wt% Ni, a total of 32% of the internal volume of the catalyst is filled with Ni_3S_2 deposits. Our finding that catalyst activity is unimpaired is thus quite striking.

To investigate catalyst deactivation at even higher deposited nickel loadings a single batch experiment, SA18-02, was run to take a charge of 100 mg of catalyst from 8 wt% Ni to 100 wt% Ni. The results of this experiment are shown in Fig. 6. The SA18-02 data resemble the data in Fig. 2 for run SA11-12 except that the rate of concentration decline is approximately 60 times

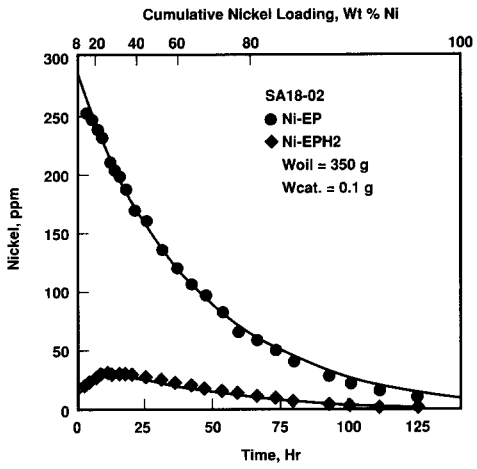

FIG. 6. Concentration versus time results for a single hydrodemetallation experiment with Ni-etioporphyrin at 320°C, 4.8 MPa H_2, on the $CoMo/Al_2O_3$ catalyst. Nickel loading on the catalyst increased from 8 wt% Ni to 100 wt% Ni during the experiment. Solid lines represent model calculations.

higher. This reflects the fact that the initial Ni-EP concentration is about 6 times higher for experiment SA18-02, and the catalyst to oil ratio is about 10 times lower. The solid curves in Fig. 6 are the best-fit model results assuming the same selectivities ($k_2/k_1 = 2.0$ and $k_3/k_1 = 4.7$). The describing rate constant k_1, at a feed concentration of 100 ppm, is 350 g oil/g cat h, the same as the mean value of the data in Fig. 5. The model based on these rate constants fits the experimental data well to deposited nickel loadings higher than 80 wt% Ni. Thus there is strong evidence that catalyst activity is maintained constant even in the presence of high nickel loadings.

Effective Diffusivity

In order to estimate the magnitude of the effective diffusivity for Ni-EP a single batch experiment, number SA15, was run with larger catalyst particles in the size range 300–350 μm (45–50 ASTM mesh). The nickel deposition profile across a typical catalyst particle from this experiment is shown in Fig. 7. The data points are electron microprobe measurements, and the solid line represents calculations made using the model of coupled multicomponent reaction and diffusion. The value of effective diffusivity, D_{eff}, used in fitting the deposition profile in Fig. 7 was 1×10^{-6} cm^2/s. This is the same value found by Agrawal and Wei (*8*) for the diffusion of Ni-EP and Ni-EPH_2 in unsulfided $CoMo/Al_2O_3$. The Thiele modulus, based on the eigenvalue λ_{slow}, which characterizes the reaction rate, is 2.8. From this we calculate an effectiveness factor, η, of 0.70. These calculations, which assume spherical particle geometry, are summarized in Table 4. We note that because these calculations are based on λ_{slow}, which reflects the observed rate of decline in nickel porphyrin concentration, they are independent of the details of our kinetic model.

This value for the effective diffusivity is compatible with our conclusion that the size of the catalyst particles used in the Ni-EP experiments discussed previously, series SA11, SA12, and SA18, was sufficiently small to ensure kinetic control and the absence of diffusional limitations. Electron microprobe analyses of sectioned catalyst particles from series SA12 and SA18, at nickel loadings of 70 wt% Ni and 100 wt% Ni, respectively, showed flat radial nickel depo-

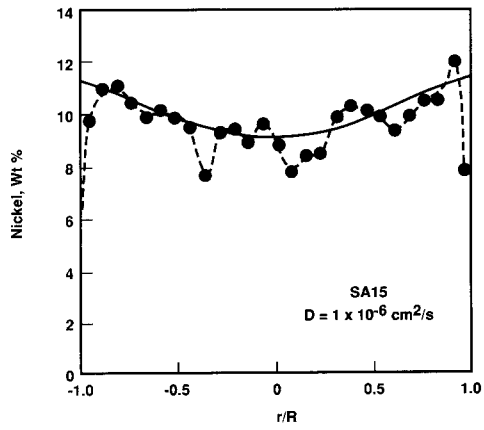

FIG. 7. Nickel deposition profile in 300-μm $CoMo/Al_2O_3$ catalyst particle. Solid line represents reaction and diffusion model calculations.

TABLE 4

Thiele Modulus and Effectiveness Factor for Diffusion-Limited HDM Series

Experimental series	Reactant	Catalyst	R (μm)	λ_{slow} (g oil/g cat h)	D_{eff} (cm^2/s)	Thiele modulus[a] ϕ	Effectiveness factor η
SA12	Ni-EP	HDS16A	40	138	1×10^{-6}	1.1	0.93
AL13	Ni-EP	HDS3 Substrate	40	14	1×10^{-6}	0.34	0.99
SA15	Ni-EP	HDS16A	150	66	1×10^{-6}	2.8	0.70
SA17	VO-EP	HDS16A	40	40	3×10^{-8}	3.3	0.63
SA18	Ni-EP	HDS16A	40	82	1×10^{-6}	0.83	0.96
SA19	VO-EP	HDS16A	20	40	3×10^{-8}	1.7	0.85

[a] Assuming ρ_{cat} = 1.49 g/ml, ρ_{oil} = 0.8 g/ml, spherical particle geometry.

sition profiles in both cases. The effectiveness factors calculated for these experimental series were 0.93 and 0.96, respectively. These calculations are also summarized in Table 4.

4. HDM OF VO-EP IN SQUALANE OVER CoMo/Al_2O_3

A single experiment (SA19) was carried out to determine VO-EP hydrodemetallation kinetics. An additional series of experiments (SA17) was carried out to examine the effective diffusivity of VO-EP and the changes in observed kinetics as vanadium-sulfide deposits accumulated on the CoMo/Al_2O_3 catalyst. The standard conditions for all experiments were 320°C, 4.8 MPa total pressure, and 14 kPa H_2S, the same standard conditions as the Ni-EP series. Initial concentrations were all in the range 90–105 ppm V, so these experiments did not probe the question of whether VO-EP HDM rate constants show a concentration dependence, as was shown to be the case for Ni-EP.

Reaction Kinetics

The hydrodemetallation of VO-EP proceeds by the same sequential mechanism as for Ni-EP, as was first reported by Agrawal and Wei (*8*). The single batch experiment (SA19), which we used to evaluate intrinsic kinetic parameters for the HDM of VO-EP, used approximately 1 g of catalyst and loaded it to approximately 4 wt% V. The catalyst particles were in the size range 37–44 μm (325–400 ASTM mesh), small enough to ensure minimal diffusion limitations. Electron microprobe analysis of sectioned catalyst particles from the run showed uniform radial vanadium deposition profiles, confirming that this experiment was carried out in the kinetic regime.

Figure 8 shows the variation in reactor concentrations as a function of time for the VO-EP kinetic experiment. As in the case of Ni-EP HDM, an initial buildup of the EPH_2 species was followed by a decline in concentration of both the EP and EPH_2 species. Comparison of Fig. 8 with Fig. 2 confirms that the overall reaction schemes were similar, but shows that the overall rate of VO-EP HDM was significantly slower than for Ni-EP. In addition, the selectivities were somewhat different for VO-EP than for Ni-EP. VO-EPH_2 built up to a concentration relative to VO-EP higher than that in the Ni-EP case, suggesting that the rates of VO-EPH_2 removal by dehydrogenation (k_2) and hydrogenolysis (k_3) were slower relative to the rate of VO-EPH_2 formation from VO-EP by hydrogenation (k_1).

The best-fit set of rate constants for SA19-01 was used to generate the solid line model results in Fig. 8. The ratio of the dehydrogenation rate constant to the hydrogenation rate constant (k_2/k_1) was found to be 1.4. The

ratio of the hydrogenolysis rate constant to the hydrogenation rate constant (k_3/k_1) was also 1.4. There is some uncertainty in these selectivities since they were estimated from a single set of data. It is clear, however, that hydrogenation of VO-EP is the rate-limiting step, and that both k_2/k_1 and k_3/k_1 are lower than in the case of Ni-EP HDM (2.0 and 4.7, respectively). The overall rate of hydrodemetallation of VO-EP is, somewhat surprisingly, slower than the HDM rate for Ni-EP. The value of the slow eigenvalue, λ_{slow}, is 40 g oil/g cat hr for VO-EP HDM, compared with a value of 230 g oil/g cat h for Ni-EP HDM at the same feed concentrations.

Catalyst Deactivation and Effective Diffusivity

The series of batch experiments, SA17, designed to examine effective diffusivity and catalyst deactivation was carried out with approximately 1 g of catalyst in the particle size range was 75–88 μm (170–200 ASTM mesh). The total vanadium loading on the catalyst at the end of the series of experiments was 25 wt% V. Because of the greater density of nickel sulfide, this is equivalent to 45 wt% nickel on the basis of equal volume of deposits.

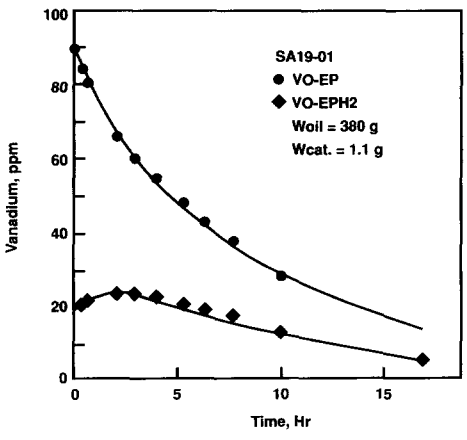

FIG. 8. Typical concentration versus time results for a single hydrodemetallation experiment with VO-etioporphyrin at 320°C, 4.8 MPa H_2, on the $CoMo/Al_2O_3$ catalyst. Solid lines represent model calculations.

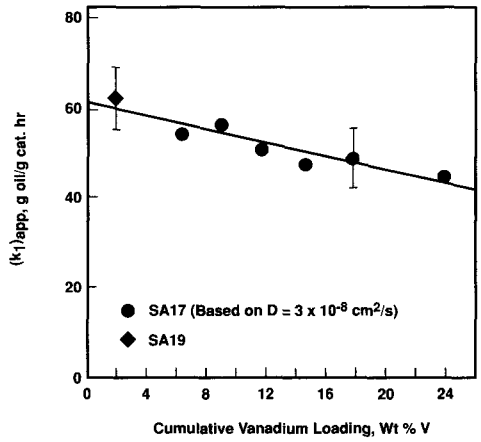

FIG. 9. Apparent hydrogenation rate constant for VO-EP hydrodemetallation, k_1, versus cumulative vanadium loading on the $CoMo/Al_2O_3$ catalyst. Conditions: 90–105 ppm V feed, 320°C, 4.8 MPa H_2.

The VO-EP HDM kinetics for each of the experiments in series SA17 were modeled assuming that the intrinsic selectivities k_2/k_1 and k_3/k_1 were both 1.4, the values found in the intrinsic kinetic experiment SA19. Figure 9 shows the fitted rate constants plotted versus cumulative vanadium loading on the catalyst. (We plot the fitted rate constant as $(k_1)_{app}$ because analysis of the vanadium deposition profiles in catalyst particles from SA17 confirmed that these experiments were run in the diffusion-limited regime.) The data in Fig. 9 show a decline in apparent catalyst HDM activity as vanadium-sulfide deposits accumulate. This decline is statistically significant at the 95% confidence interval. At a deposited vanadium loading of 25 wt% V, the value for $(k_1)_{app}$ is 30% lower than that found with the fresh catalyst. Possible interpretations of this result are: (1) that the effective diffusivity is constant throughout the series of experiments and a lower activity of the deposited vanadium sulfide relative to the fresh catalyst is causing a decline in observed catalyst activity, or (2) that the intrinsic activity of the catalyst is maintained as vanadium-sulfide deposits accumulate, and that instead deactivation can be attributed to a decline in effective

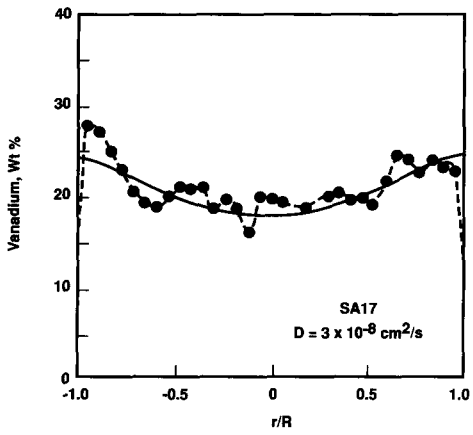

FIG. 10. Vanadium deposition profile in 80-μm $CoMo/Al_2O_3$ catalyst particle. Solid line represents reaction and diffusion model calculations.

diffusivity. These experiments do not provide a basis for distinguishing between these possibilities, and this question warrants further investigation.

Figure 10 shows the profile of vanadium deposition in a typical catalyst particle from run SA17 as determined by electron microprobe analysis. It is clearly not flat, confirming that the VO-EP HDM reactions were diffusion-limited. The solid curve in Fig. 10 is the vanadium deposition profile predicted by the theory of coupled multicomponent reaction and diffusion. The value of D_{eff} for VO-EP and $VO\text{-}EPH_2$ that fits the measured end-of-series vanadium deposition profile is 3×10^{-8} cm^2/s. The Thiele modulus calculation for SA17 is summarized in Table 4. The calculated Thiele modulus is 3.3 and the effectiveness factor is 0.63.

The value of the effective diffusivity, 3×10^{-8} cm^2/s, is significantly lower than the value on the order of 1×10^{-6} cm^2/s found by Agrawal and Wei (*8*) for VO-EP in unsulfided $CoMo/Al_2O_3$. A possible explanation for this result comes from the interaction between the vanadyl group and the sulfided catalyst. This explanation is discussed further in Section 6.

5. HDM OF Ni-EP IN SQUALANE OVER A LOW-PROMOTER ALUMINA CARRIER

We carried out a series of experiments (SA13) with a low-promoter alumina carrier to investigate Ni-EP hydrodemetallation kinetics and the effect of accumulated nickel-sulfide deposits. The alumina carrier actually contained small quantities of molybdenum, cobalt, nickel, and phosphorous. Its properties are summarized in Table 2. Reactor conditions for the HDM experiments were the same as those used in previous experiments, 320°C and 4.8 MPa total pressure, but the hydrogen sulfide partial pressure was somewhat lower at 1–7 kPa (0.02–0.15 vol%). The alumina carrier was presulfided in the reactor, according to the standard procedure used for the $CoMo/Al_2O_3$ catalyst. The particles were in the size range 75–88 μm (170–200 ASTM mesh). Electron microprobe analysis confirmed that the nickel deposition profile was flat, meaning that the kinetic experiments were carried out in the absence of diffusion limitations. Table 4 summarizes Thiele modulus calculations that support this finding, assuming the same effective diffusivity for Ni-

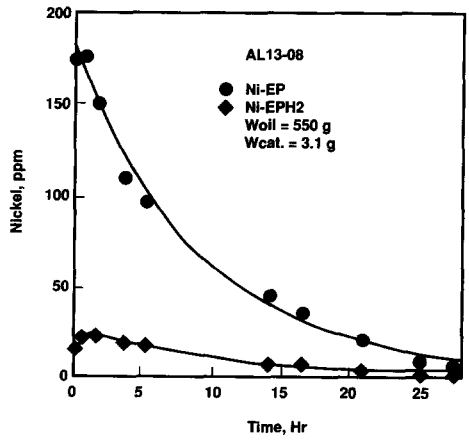

FIG. 11. Typical concentration versus time results for a single hydrodemetallation experiment with Ni-etioporphyrin at 320°C, 4.8 MPa H_2, on the low-promoter alumina carrier. Solid lines represent model calculations.

EP and Ni-EPH_2 in this catalyst as in the $CoMo/Al_2O_3$ catalyst.

Reaction Kinetics

Figure 11 shows the variation in reactor concentrations as a function of time for a typical experiment. It is very similar to Fig. 2, which was carried out over the $CoMo/Al_2O_3$ catalyst, except that the time scale is much longer. This suggests that the HDM reaction selectivities over the two catalysts were similar but that the activity of the alumina carrier was much lower. The solid lines in Fig. 11 are model calculations, assuming the same selectivities as for the $CoMo/Al_2O_3$ catalyst ($k_2/k_1 = 2.0$ and $k_3/k_1 = 4.7$).

Catalyst Deactivation

Seven consecutive experiments were run on the alumina carrier. Figure 12 shows the hydrogenation rate constant, k_1, for each experiment plotted versus cumulative nickel loading. The slope of a line regressed through the data does not differ significantly from zero, at the 95% confidence interval. This means that the HDM activity of the alumina carrier remained constant in the presence of up to 25 wt% Ni. We describe the data with the mean value for k_1, which is 26 g oil/g cat h at a feed concentration of 100 ppm Ni.

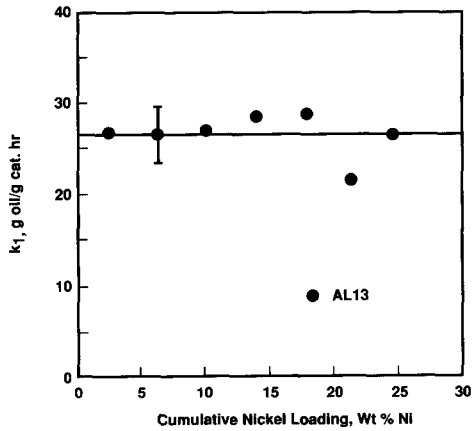

FIG. 12. Hydrogenation rate constant for Ni-EP hydrodemetallation, k_1, versus cumulative nickel loading on the low-promoter alumina carrier. Rate constant adjusted to initial Ni-EP concentration of 100 ppm Ni. Conditions: 100 ppm Ni feed, 320°C, 4.8 MPa H_2.

TABLE 5

Comparison of the Low-Promoter Alumina Carrier and the $CoMo/Al_2O_3$ Catalyst

	Value in the alumina carrier relative to the $CoMo/Al_2O_3$ catalyst
Promoters	
Molybdenum	2%
Total promoter (Ni + Co + Mo)	7%
Phosphorous	4%
Ni-EP Hydrogenation rate constant (k_1)	7%

Comparison of the Low-Promoter Alumina Carrier and the $CoMo/Al_2O_3$ Catalyst

The two catalysts tested for Ni-EP HDM are similar in that both showed constant activity and selectivity as deposited nickel levels were increased. Neither catalyst showed a loss or increase in activity. The selectivities of the two catalysts for hydrogenation, dehydrogenation, and hydrogenolysis were the same. However, the activity of the alumina carrier was about 7% of that of the $CoMo/Al_2O_3$ catalyst, on an equivalent surface area basis. As shown in Table 5, this result matches the lower-promoter levels of the alumina carrier. The significance of these results is discussed further in Section 6.

6. DISCUSSION

6.1. Etioporphyrin Reactivities and Diffusivities

We found both the reactivity and the diffusivity of VO-EP to be significantly lower than those of Ni-EP. The value of the intrinsic hydrogenation rate constant, k_1, for VO-EP was lower than the value for Ni-EP by a factor of about 5. The value of the apparent effective diffusivity for VO-EP was lower than the value for Ni-EP by a factor of 30.

Although it is generally accepted that

when both species are present, vanadyl compounds are more reactive than nickel compounds under hydrodemetallation conditions, our result that the single species VO-EP reactivity is lower than that of single species Ni-EP has precedent. Hung and Wei (*7*), working with the unsulfided CoMo/Al_2O_3 catalyst, found the HDM rate of VO-EP to be lower than that of Ni-EP at temperatures below 320°C. Model compound studies by Rankel (*23*) also showed a temperature dependence of relative V and Ni HDM rates.

Our results showed that, for both Ni-EP and VO-EP, the overall rate of hydrodemetallation was significantly faster on the sulfided CoMo/Al_2O_3 catalyst than on the unsulfided catalyst. This result is in keeping with results reported by Ware and Wei (*11*) for another porphyrin, Ni-T3MPP. For Ni-EP, we found the rate-limiting hydrogenation step (k_1) was increased by a factor of 8 on the sulfided catalyst. In addition the reaction selectivity was shifted in favor of hydrogenolysis, with a 30-fold increase in the metal deposition step (k_3). For VO-EP, we found the rate-limiting hydrogenation step (k_1) was increased by a factor of 5 on the sulfided catalyst. The reaction selectivity was not affected significantly.

The value for the effective diffusivity of Ni-EP in the sulfided catalyst, 1×10^{-6} cm^2/s, is consistent with the value found previously for the unsulfided catalyst (*8*). However, the apparent diffusivity of VO-EP, 3×10^{-8} cm^2/s, is lower by a factor of 30 than that observed on the unsulfided catalyst. A low effective diffusivity for vanadyl porphyrins in the sulfided catalyst has been observed previously by West (*24*) who used a reaction system similar to the one used in this work, and calculated an apparent effective diffusivity for VO-TPP of 2×10^{-7} cm^2/s from vanadium deposition profiles. Since the molecular size of the nickel and vanadyl porphyrins is essentially the same, we must look to interaction effects to explain the difference in diffusivities. One possibility is that the high electron density associated with the vanadyl ligand encourages interactions between the porphyrin and oil components or impurities, increasing the effective molecular size. However, this hypothesis is inconsistent with previous results, since no reduction in VO-EP effective diffusivity relative to Ni-EP was observed in the unsulfided catalyst system (*8*). Another possible hypothesis, more consistent with the experimental evidence, is that VO-EP adsorbs on the surface of the sulfide CoMo/Al_2O_3 catalyst, reducing the apparent effective diffusivity.

Weisz (*25*) has developed a general approach for interpreting the apparent diffusivities from diffusion-controlled adsorption processes. He shows that the relationship between the apparent diffusivity, D_{app}, and the true diffusivity, D, is derivable within about ±30% even for the extreme cases of a "weak" linear isotherm and a "strong" irreversible sorption. The applied correction is c_f/c_0, which is the ratio of the total final concentration adsorbed on the solid volume, c_f, when equilibrated to the external driving concentration, c_0. The result given by Weisz is

$$D_{app} = \gamma \frac{\tau}{\Psi_{eff}} \frac{c_f}{c_0} D, \qquad (8)$$

where τ is a tortuosity factor, ψ_{eff} is the fractional volume in which diffusion occurs, and γ has a value between $\gamma = 1.0$ and $\gamma = 1.6$, depending on the nature of the adsorption isotherm. Weisz and Zollinger (26) used Eq. (8) to show that adsorption effects accounted for the experimental observation that the apparent diffusivities of dye molecules in a transient sorption–diffusion system were up to two orders of magnitude lower than the expected values for diffusion in the solvent.

The approach taken by Weisz provides a basis for interpreting the apparently low diffusivity for VO-EP in the sulfided CoMo/Al_2O_3 catalyst. The ratio c_f/c_0 would have to be at least 30 at reaction conditions to explain the low apparent diffusivity. This ratio implies high coverage of the adsorbed VO-

EP on the catalyst surface. In contrast the Ni-EP diffusivity results suggest a lower equilibrium adsorption coverage by this porphyrin. To be consistent with these results, we would expect the VO-EP HDM reaction rate constants to display concentration dependence in the same manner as has been observed for Ni-EP. Morales and co-workers (*27, 28*) have examined the interaction of vanadyl porphyrins extracted from Boscan crude with $CoMo/Al_2O_3$ catalysts. They find evidence for strong adsorption on sulfided and reduced catalysts where adsorption results from electron donation from the surface, and weaker interaction on oxide catalysts. Galiasso and Morales (*29*), however, report reduced adsorption of vanadyl porphyrins at elevated temperatures.

6.2. Catalyst Deactivation

Both the sulfided $CoMo/Al_2O_3$ catalyst and the low-promoter alumina carrier neither deactivated nor acquired catalytic activity as nickel-sulfide deposits accumulated. In fact, catalyst activity levels proportional to the original promoter loadings were maintained in the presence of relatively high deposit loadings on the two very different catalysts. These results are inconsistent with a uniform nickel-sulfide deposition model, in which deposits are built up in a layer-by-layer manner, masking the fresh catalyst surface after the deposition of just one monolayer. (This assumption has been made frequently in modeling the deactivation of hydroprocessing catalysts (*30–32*).) Rather, they are consistent with a mode of nickel-sulfide deposition by which the active components of the catalyst can continue to make a significant contribution to HDM activity, even in the presence of high levels of deposited nickel sulfides. A number of hypotheses by which the cobalt–molybdenum active sites on the fresh catalyst are continuously regenerated or remain uncovered have been proposed. Possible mechanisms include migration of the deposited metal sulfides to the free alumina support (*4*), migration of the Co–Mo–S to the top of the deposited layer (*33*), or the spatially nonuniform deposition of the metal sulfides (*34, 35*). The catalyst characterization studies presented in the following paper (*18*) address the question of the morphology and dispersion of the metal-sulfide deposits further.

Studies with petroleum feeds have suggested that aluminas acquire catalytic activity for removing metals from a residual feedstock when exposed to the feedstock under hydroprocessing conditions (*2, 6, 36*). Takeuchi *et al.* (*6*) report that the HDM activity of a bare carrier increases 10-fold with the deposition of 15 wt% vanadium, to become comparable to that of a $CoMo/Al_2O_3$ or $NiMo/Al_2O_3$ catalyst. In contrast, our results show no change in the activity of the alumina carrier with the deposition of 25 wt% nickel. (Although Takeuchi *et al.* report the metal loading on the catalyst in wt% vanadium, the study was conducted with a heavy petroleum oil which presumably contained nickel as well as vanadium.) One difference between the industrial results, which show activation of alumina carriers with metal deposition, and our model compound studies, is that no vanadium was present in our alumina carrier studies. Vanadium sulfides, or mixed nickel and vanadium sulfides, whose HDM catalytic activity have not been examined in the model compound studies, may be responsible for the industrial results.

Previously we have reported HDM catalyst deactivation experiments using the same $CoMo/Al_2O_3$ catalyst used for the studies reported here, with nickel etioporphyrin as reactant, and Kaydol, a commercial mineral oil, as solvent (*34*). These experiments showed apparent deactivation of the catalyst as nickel-sulfide deposits accumulated on the catalyst, in contrast to the experiments using squalane reported here in which no deactivation is observed. Further experimental work to investigate this discrepancy is reported by Smith (*15*). The conclusion of these studies is that the apparent deactivation in the Kaydol experiments is

due to some effect other than the accumulation of metal deposits on the catalyst. We hypothesize that the accumulation in the batch reactor of Kaydol reaction products, possibly polynuclear aromatic hydrocarbons, which adsorb competitively with the Ni-EP and Ni-EPH_2, were the cause of the apparent deactivation.

Neither the nickel nor the vanadium catalyst aging experiments show an initial deactivation period. However, our experimental approach was not sensitive to very rapid initial deactivation effects, so our results do not address the possibility of rapid site poisoning by deposited metal sulfide at loadings less than 1 wt% metal. In addition, our results do not address the questions of coking or competitive adsorption effects. Since the level of carbonaceous deposits accumulated on the catalysts in our experiments is relatively low, about 5 wt%, we used a clean model-compound reactant system. Further work is warranted to examine these questions.

7. CONCLUSIONS

(1) At conditions of temperature in the range 280–350°C and at a total pressure of 4.8 MPa, the hydrodemetallation of Ni-EP and VO-EP proceeded by the same consecutive mechanism on a sulfided $CoMo/Al_2O_3$ catalyst as had been observed previously for an unsulfided $CoMo/Al_2O_3$ catalyst (*8*). Reaction occurred via a reversible hydrogenation step to a stable etiochlorin intermediate, and then via a faster metal deposition step. The individual steps in the Ni-EP hydrodemetallation sequence had temperature dependencies similar to those reported by Agrawal and Wei (*8*) for the unsulfided catalyst.

(2) Nickel etioporphyrin in squalane hydrodemetallation studies carried out in a batch reactor at 320°C, 4.8 MPa hydrogen, 14 kPa hydrogen sulfide showed that, contrary to expectations, sulfided $CoMo/Al_2O_3$ catalysts operating in the kinetic regime did not deactivate significantly as they accumulated nickel-sulfide deposits to levels as high as 100 wt% Ni, the equivalent of more than three monolayers.

(3) Equivalent Ni-EP HDM studies carried out with a low-promoter alumina carrier showed that the carrier had a low level of catalytic activity, about 7% of the activity of the $CoMo/Al_2O_3$ catalyst on an equivalent surface area basis. This level of HDM activity is approximately proportional to (Co,Ni)MoS_2 and P promoter loadings.

(4) Both the sulfided $CoMo/Al_2O_3$ catalyst and the low-promoter alumina carrier neither deactivated nor acquired catalytic activity as nickel-sulfide deposits accumulated. The relative activity for the two catalysts matched the relative promoter loadings. These observations are consistent with a mode of nickel-sulfide deposition by which the active components of the catalyst continued to make a significant contribution to HDM activity, even in the presence of high levels of deposited nickel sulfides. They are inconsistent with the model of a rapid initial deactivation of the catalyst due to site poisoning by the deposited nickel sulfide.

(5) Vanadyl etioporphyrin in squalane HDM studies carried out at the same conditions of temperature and pressure as the Ni-EP HDM studies, on equivalently sized $CoMo/Al_2O_3$ catalyst particles, were diffusion-limited. Examination of the reaction and diffusion parameters showed that the controlling parameter for this effect is the very low effective diffusivity of VO-EP. The observed deactivation of the catalyst as vanadium-sulfide deposits accumulated in these experiments is consistent with the generally accepted hypothesis that the accumulation of metal-sulfide deposits in catalyst pores is responsible for the relatively slow, steady deactivation that characterizes the intermediate period of the life of a hydroprocessing catalyst. However, our results do not allow us to distinguish between kinetic and transport effects in this deactivation regime.

(6) Both the reactivity and the apparent effective diffusivity of VO-EP on the sulfided catalyst were found to be significantly lower than those of Ni-EP, at 320°C, 4.8 MPa hydrogen, 14 kPa hydrogen sulfide. The reactivity was lower by a factor of 5, and the apparent diffusivity by a factor of 30.

APPENDIX: NOMENCLATURE

c_f	Total final concentration adsorbed on the solid (Eq. (8))
c_0	External driving concentration (Eq. (8))
C	Concentration
$\mathbf{C}$	Concentration matrix
$\mathbf{C_0}$	Initial concentrations
D	Diffusivity
D_{app}	Apparent diffusivity
D_{eff}	Effective diffusivity
HDM	Hydrodemetallation
k_1	Hydrogenation rate constant
k_{1s}	Surface reaction rate constant
k_2	Dehydrogenation rate constant
k_3	Hydrogenolysis rate constant
$\mathbf{K}$	Rate matrix
M_0	Initial porphyrin concentration (Ni-EP + Ni-EPH_2)
Ni-EP	Nickel etioporphyrin
Ni-EPH_2	Nickel etiochlorin
Ni-T3MPP	Nickel tetra (3-methylphenyl)porphyrin
P_{H_2}	Hydrogen pressure
r	Radius
R	Radius of the catalyst particle
S_0	Total number of active sites
t	Time
$\hat{t}$	Contact time (Eq. (1))
VO-EP	Vanadyl etioporphyrin
VO-EPH_2	Vanadyl etiochlorin
W_c	Weight of catalyst
W_{oil}	Weight of oil in the reactor
$\mathbf{X}$	Eigenvector matrix of the rate matrix $\mathbf{K}$

Greek

ϕ	Thiele modulus
γ	Correction factor in Eq. (8), whose value depends on the strength of the adsorption isotherm
η	Effectiveness factor
λ_i	Eigenvalues of the rate matrix, $\mathbf{K}$
ρ_{oil}	Oil density
ρ_{cat}	Catalyst density
τ	Tortuosity
Ψ_{eff}	Fractional catalyst volume in which diffusion occurs

ACKNOWLEDGMENTS

The authors are grateful to the following people for their assistance: Erja Rautiainen of Neste Oy, Finland, for extensive help with the hydrodemetallation experiments; Hervé Toulhoat, Raymonde Szymanski and the electron microscopy section at the Institut Français du Pétrole in Reuil-Malmaison, France, for the electron microprobe analyses; and Chi-Wen Hung of Chevron Research Company, Bob Ware of Mobil Oil Research and Development Corporation, and Ian Webster of Unocal Corporation for helpful discussions.

REFERENCES

1. Beuther, H., and Schmid, B. K., *Proc. 6th World Petrol. Congr.* Sect. III, Paper 20 (1963).
2. Sie, S. T., *in* "Catalyst Deactivation" (B. Delmon and G. F. Froment, Eds.), Vol. 6, p. 545. Elsevier, Amsterdam, 1980.
3. Dautzenberg, F. M., Van Klinken, J., Pronk, K. M. A., Sie, S. T., and Wijffles, J. B., *Chem. React. Eng. Cong.* **21,** 254 (1981).
4. Pazos, J. M., Gonzalez, J. C., and Salazar-Guillen, A. J., *Ind. Eng. Chem. Process Des. Dev.* **22,** 653 (1983).
5. Tamm, P. W., Harnsberger, H. F., and Bridge, A. G., *Ind. Eng. Chem. Process Des. Dev.* **20,** 262 (1981).
6. Takeuchi, C., Asoka, S., Nakata, S., and Shiroto, Y., *ACS Prepr. Div. Petrol. Chem.* **30**(1), 96 (1985).
7. Hung, C. W., and Wei, J., *Ind. Eng. Chem. Process Des. Dev.* **19,** 250–257 (1980).
8. Agrawal, R., and Wei, J., *Ind. Eng. Chem. Process Des. Dev.* **23,** 505–515 (1984).
9. Rankel, L. A., and Rollman, L. D., *Fuel* **62**(1), 44 (1983).
10. Weitkamp, J., Gerhardt, W., and Scholl, D., *in*

"Proceedings, 8th International Congress on Catalysis, Berlin 1984" Vol. 2, p. 269. Dechema, Frankfurt-am-Main, 1984.
11. Ware, R. A., and Wei, J., *J. Catal.* **93,** 100–135 (1985).
12. Webster, I. A., Sc.D. thesis, Massachusetts Institute of Technology, 1984.
13. Chen, H. J., and Massoth, F. E., *Ind. Eng. Chem. Res.* **27,** 1629 (1988).
14. Quann, R. J., Ware, R. A., Hung, C. H., and Wei, J., *Adv. Chem. Eng.* **14,** 95 (1988).
15. Smith, B. J., Sc.D. thesis, Massachusetts Institute of Technology, 1988.
16. Limbach, K. W., Ph.D. thesis, Massachusetts Institute of Technology, 1989.
17. Rautiainen, E. P. H., and Wei, J., *Chem. Eng. Commun.* **98,** 113 (1990).
18. Smith, B. J., and Wei, J., *J. Catal.* **132,** 21 (1991).
19. Wei, J., and Wei, R. G., *Chem. Eng. Commun.* **13,** 251 (1982).
20. Moler, C., Little, J., and Bangert, S., "PC MATLAB User's Guide" The MathWorks, Portola Valley, 1985.
21. Wei, J., *J. Catal.* **1,** 526 (1962).
22. Agrawal, R., Sc.D. thesis, Massachusetts Institute of Technology, 1980.
23. Rankel, L. A., *ACS Div. Petrol. Chem.* **26** (3), 689 (1981).
24. West, M., Ph.D. thesis, University of California, Berkeley, 1983.
25. Weisz, P. B., *Trans. Faraday Soc.* **63,** 1801 (1967).
26. Weisz, P. B., and Zollinger, H., *Trans. Faraday Soc.* **63,** 1815 (1967).
27. Morales, A., and Galiasso R., *Fuel* **61,** 13 (1982).
28. Morales, A., Garcia, J. J., and Prada, R., *in* "Proceedings, 8th International Congress on Catalysis, Berlin, 1984," Vol. 2, p. 341. Dechema, Frankfurt-am-Main, 1984.
29. Galiasso, R., and Morales, A., *Appl. Catal.* **74,** 57 (1983).
30. Rajagopalan, K., and Luss, D., *Ind. Eng. Chem. Process Des. Dev.* **18**(3), 459 (1979).
31. Khang, S. J., and Mosby, J. F., *Ind. Eng. Chem. Process Des. Dev.* **25,** 437 (1986).
32. Limbach, K. W., and Wei, J., *AIChE J.* **34**(2), 305 (1988).
33. Fleisch, T. H., Meyers, B. L., Hall, J. B., and Ott G. L., *J. Catal.* **86,** 147 (1984).
34. Smith, B. J., and Wei, J., "Catalyst Deactivation during the HDM of Ni Porphyrin over CoMo/Al_2O_3," presented at the AIChE National Meeting, November 10–15, Chicago, IL, 1985.
35. Wei, J., *in* "Catalyst Design: Progress and Perspectives" (L. L. Hegedus, Ed.), p. 245. Wiley, New York, 1987.
36. Devanneaux, J., Gallex, J. P., and Engelhard, P. A., *ACS Prepr. Div. Petrol. Chem.* **30**(1), 84 (1985).